



Numerical estimation of photon reabsorption process and optical crosstalk in arrays of HgCdTe photodiodes

A. Jóźwikowska¹ · K. Jóźwikowski² 

Received: 29 November 2018 / Accepted: 12 February 2019 / Published online: 7 March 2019
© The Author(s) 2019

Abstract

The effect of photon reabsorption (recycling) on photoelectric parameters of non-equilibrium P⁺nN⁺ photodiodes, for example the pixels of the detector array, was analyzed. We solved the system of transport equations additionally extended by two balances equations for photons. It was shown that the density of photons in photodiodes is strongly dependent on the concentration of charge carriers. This phenomenon results in a drastic reduction in the rate of radiative recombination and generation in analyzed photodiodes. Additionally, the phenomenon of optical crosstalk between the nearest pixels in the matrix was examined. The increase in the dark current caused by this phenomenon was estimated. It depends on the size of the pixel, the distance between pixels, and the value of bias voltage. The increase in the current is around 0.5% for a pixel with surface $10 \times 10 \mu\text{m}^2$, and around 1% for one with $5 \times 5 \mu\text{m}^2$, both reverse biased with 0.2 V.

Keywords Non-equilibrium mode of operation · HgCdTe photodiodes · Reabsorption effect · Optical crosstalk

1 Introduction

Numerical modeling of photoelectric phenomena enables the design of infrared detectors with a complicated internal structure whose technical parameters are in good agreement with the theoretical values. To achieve such a consistency, it is necessary to include in the simulations as many different generation and recombination mechanisms

This article is part of the TopicalCollection on Numerical Simulation of Optoelectronic Devices, NUSOD' 18.

Guest edited by Paolo Bardella, Weida Hu, Sławomir Sujecki, Stefan Schulz, Silvano Donati, Angela Traenhardt.

✉ K. Jóźwikowski
krzysztof.jozwikowski@wat.edu.pl

¹ Faculty of Applied Informatics and Mathematics, Warsaw University of Life Science, Nowoursynowska 166 St., 02-787 Warsaw, Poland

² Institute of Applied Physics, Military University of Technology, Gen. Urbanowicza 2 St., 00-908 Warsaw, Poland

as possible, and to use correct relationships. In CdHgTe, thermal G–R processes determined by inter band mechanisms, Auger1 (A1) Auger 7 (A7) and radiative mechanism (R), are critical. Continuous progress in the technology of growth of the heterostructures results in lower significance of SHR mechanisms related to metal vacancies and dislocations. Nevertheless, the SHR mechanisms still play a significant role. In the programs developed by us, we have also considered the tunnel generation and impact ionizations, although for the detectors considered in this work, they have practically no significance. Among researchers there are controversies regarding the radiative mechanism. (Van Roosbroeck and Shockley 1954) derived dependencies on the radiative generation and radiation rates, but the photons' densities present in their relationships are densities in the thermal equilibrium described by the Planck distribution. Humphreys (1983, 1986) noticed that their expression on the radiative generation rate is not valid in non-equilibrium conditions. The energetic coupling between photons and charge carriers causes photon densities to be related to the concentrations of charge carriers. In addition, the process of secondary absorption (recycling) of photons previously generated in the radiative recombination (RR) process of electron–hole pairs should be considered. In 2012, we expanded the method developed by Humphreys and used it to analyze G–R processes in a photodiode built from HgCdTe heterostructure (Jóźwikowski et al. 2012).

In our method we treat photons as the Einstein gas of particles described by the Bose–Einstein statistic. Next, using the method proposed by Humphreys (1983, 1986), we divide photons into two groups in specific energy ranges to determine the average values of the absorption coefficient and the radiative generation factor for them. We consider additional effects accompanying the radiative generation (RG) and (RR) phenomenon, i.e. recycling of photons generated by RR (Jóźwikowski et al. 2011, 2012), and the spatially changing non-equilibrium photons density. This effectively changes the values of RR and RG rates, which are different from those obtained by (Van Roosbroeck and Shockley 1954). Correct estimation of these parameters is very important for those cases where the A1 and A7 processes cease to dominate. However, after illuminating the pixel the emission of secondary photons by the detector caused by the acts of RR may trigger an unfavorable effect of the so-called optical crosstalk, which generates a false signal in neighboring pixels of the detector array. This phenomenon is a bane for constructors of detector matrices, and it becomes increasingly important as pixels in matrices are getting smaller and smaller (the surface area reaches the size of just $5 \times 5 \mu\text{m}^2$), and the distances between pixels are of the order of one micrometer. The motivation to do this work was the need to analyze the impact of non-equilibrium photons on single-pixel photoelectric parameters and optical crosstalk in a detector array.

To this end, we improved the earlier model presented in Jóźwikowski et al. (2011, 2012) and used it to determine the parameters of thermoelectrically cooled long wavelength infrared (LWIR) HgCdTe photodiodes in non-equilibrium mode of operation (NEMO). There is an intense ongoing research on such detectors, in which it is possible to suppress Auger processes without the need for cryogenic cooling. Therefore, it is important to assess what is the actual participation in the G–R processes of the R mechanism, which may dominate in these conditions. In addition, we showed how to estimate the optical cross-talk in the matrixes of such detectors. So far, it has not been possible to construct large matrices built of non-equilibrium detectors. However, constant advances in technology should allow to eliminate the heterogeneities and instabilities associated with quite a significant polarization of individual pixels, which is a major obstacle to their implementation. The results obtained in this work should be useful for the designers of non-equilibrium detector matrices, and the presented method can be also applied

for other types of detectors. Despite the theoretical character of this work, our programs and methods have been verified on numerous occasions by analyzing the parameters of the detectors manufactured in Vigo-System SA, obtaining a good compliance with the measurement (for example Józwickowski et al. 2010, 2017a, b).

2 Numerical method and results

To solve the problem of optical crosstalk and photons reabsorption phenomenon we consider equations additional to the standard set of carrier transport equations. These equations, named the transport equations for photons were presented in our previous works (Józwickowski et al. 2011, 2012), and are related to the carrier transport equations through the inter-band radiative GR mechanism and by the equation of energy balance. The equation of energy balance (Eq. 5) has been now modified by us and expanded to consider the participation of photons. As a result, we have the full energy coupling between the photons and current carriers in the semiconductor structure. Our calculations give results that differ from those in Józwickowski et al. (2011, 2012). The transport equation for photons of density q^i , for which the energy $E^i < h\nu \leq E^i + \Delta E^i$ is expressed by:

$$\frac{\partial q^i}{\partial t} = G_{RAD}^i \frac{np}{n_0 p_0} - q^i \alpha^i \frac{c}{\eta_i} - \nabla j_{q^i} \tag{1}$$

where $G_{RAD}^i = \int_{E^i}^{E^i + \Delta E^i} \frac{c q_0^i(\nu) \alpha(\nu)}{\eta(\nu)} d\nu$, $\alpha(\nu)$ is the absorption coefficient, and the current density of i -th kind photons reads $j_{q^i} = q^i c / 4 \eta_i^3$. Following Humphreys (1983, 1986), the quantities in Eq. 1 can be expressed by appropriate averages

$$q_0^i = \int_{E^i}^{E^i + \Delta E^i} f(\nu) d\nu \tag{2}$$

$$\frac{\alpha^i}{\eta^i} = \frac{1}{q_0^i} \int_{E^i}^{E^i + \Delta E^i} \frac{f(\nu) \alpha(\nu)}{\eta(\nu)} d\nu \tag{3}$$

$$\bar{E}_{q^i} = \frac{1}{q_0^i} \int_{E^i}^{E^i + \Delta E^i} f(\nu) h\nu d\nu \tag{4}$$

Here h is the Planck constant, $f(\nu)$ is the Planck distribution function at thermal equilibrium, ν is the photon frequency. Other symbols in Eqs. (1)–(5) are: indexes p and n refer to holes and to electrons, respectively, index 0 denotes the thermal equilibrium, c is the speed of light, η the refractive index, ∇ gradient, e is the elementary charge, C_V the specific heat, ζ is the coefficient of thermal conductivity, ρ_s denotes the density of entropy, μ is the mobility and j is the current density. Using the iterative methods, we solve the set of transport equations for electrons and holes, together with the Poisson equation, transport equations for photons (Eq. 1) and energy balance (Eq. 5), obtaining the spatial distribution of quasi Fermi energies Φ_n and Φ_p , electric potential Ψ , temperature T and density of photons q^i . The equation for energy balance reads:

$$C_V \frac{\partial T}{\partial t} = -\nabla(\zeta \nabla T) - \nabla \left(\rho_{s_p} \mu_p \nabla \Phi_p + \rho_{s_n} \mu_n \nabla \Phi_n \right) - \nabla(\Phi_n j_e + \Phi_p j_p) + \sum_i \left(q_0^i \frac{\alpha^i}{\eta^i} c \frac{np}{n_0 p_0} - q^i \alpha^i \frac{c}{\eta_i} \right) \bar{E}_{q_i} \tag{5}$$

The set of transport equations includes also the balance equation for electrons (Eq. 6) and for holes (Eq. 7)

$$\frac{\partial n}{\partial t} = \frac{1}{e} \nabla j_n + (G - R)_{NR} - \sum_i q_0^i \frac{\alpha^i}{\gamma_i} c \frac{np}{n_0 p_0} + \sum_i q^i \frac{\alpha^i}{\gamma_i} c \tag{6}$$

$$\frac{\partial p}{\partial t} = -\frac{1}{e} \nabla j_p + (G - R)_{NR} - \sum_i q_0^i \frac{\alpha^i}{\gamma_i} c \frac{np}{n_0 p_0} + \sum_i q^i \frac{\alpha^i}{\gamma_i} c \tag{7}$$

and the Poisson’s equation reads as

$$\nabla^2 \Psi = -\frac{e}{\epsilon \epsilon_0} (N_D^+ - N_A^- + p - n) - \frac{1}{\epsilon} \nabla \Psi \nabla \epsilon. \tag{8}$$

Here ϵ is the static dielectric constant, $\bar{E}_{q_i} = \frac{1}{q_0^i} \int_{E^i}^{E^i + \Delta E^i} \frac{\partial q_0(v)}{\partial v} h\nu dv$ is the average energy of photons from the energy range ΔE^i , $\frac{\partial q_0(v)}{\partial v}$ is the Planck distribution function, density of photons is $q_0^i = \int_{E^i}^{E^i + \Delta E^i} \frac{\partial q_0(v)}{\partial v} dv$, $j_e = n\mu_n \nabla \Phi_n + \rho_{s_n} \mu_n \nabla T$, $j_p = p\mu_p \nabla \Phi_p + \rho_{s_p} \mu_p \nabla T$

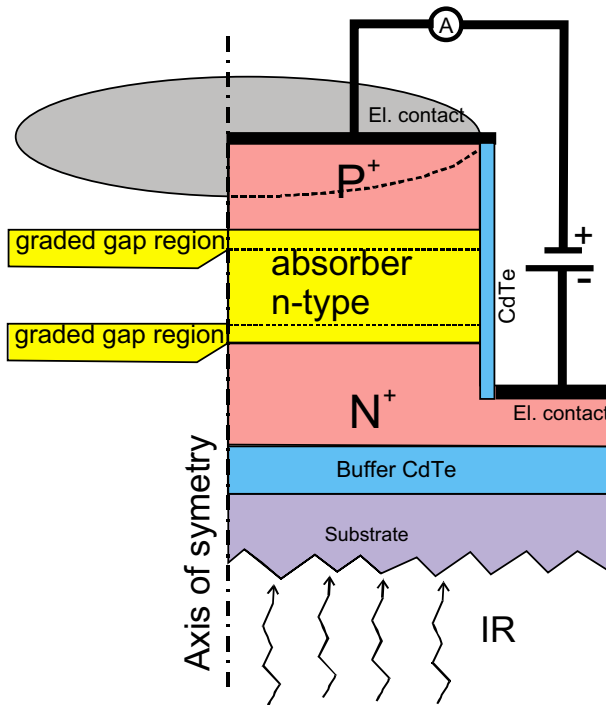


Fig. 1 Thermoelectrically cooled LWIR HgCdTe photodiodes working in non-equilibrium mode of operation (NEMO)

Fig. 2 Spatial distribution (along the axis of symmetry) of doping and mole fraction in pixel. (At T = 150 K mole fraction in absorber region $x = 0.2$, at 230 K $x = 0.183$)

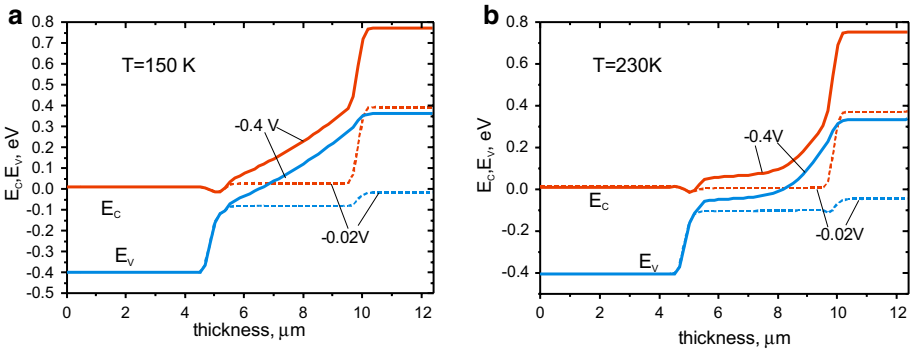
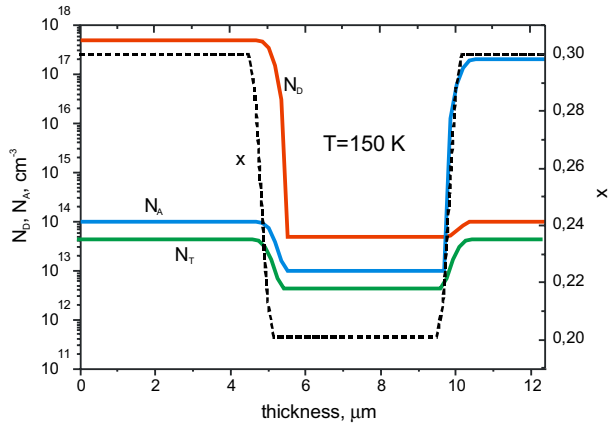


Fig. 3 Spatial distribution of the band structure with arbitrary chosen a bias voltage

(Józwikowski et al. 2015) and ζ is the coefficient of thermal conductivity, and $(G-R)$ is the total net non-radiative generation rate. Here we have distinguished 2 types of averages \bar{E}_{q^i} in energy ranges $E_G(abs.) \leq E_{q^1} < E_G(N^+, P^+)$ and $E_{q^2} \geq E_G(N^+, P^+)$, however, the number of averages may be increased depending on one's needs. E_G is the energy gap, and index *abs* denotes the absorber. N^+, P^+ are regions presented in Fig. 1, α^i is the average absorption coefficient for photons associated in the specified energy range, and $(G - R)_{NR}$ denotes the thermal net generation rate determined by non-radiative processes.

Solving the set of transport equations, we will obtain the spatial distributions of temperature T , quasi Fermi energies Φ_n and Φ_p , electrical potential Ψ , as well as photon density q^1 and q^2 . Having these we can determine all physical quantities occurring in transport process in a heterostructure.

We have analyzed the LWIR P^+vN^+ cylindrical mesa photodiodes working at 150 K and 230 K. The architecture of the half cross-section of these structures is shown in Fig. 1. Figures 2, 3, 4, 5 and 6 show spatial distributions of different physical quantities along the axis of symmetry marked in Fig. 1. Figure 2 presents spatial distribution of mole fraction x , donor concentration N_D , acceptor concentration N_A and concentrations of metal vacancies N_T in structure working at 150 K. The photodiode operating in 230 K has a different mole fraction in the absorber area ($x = 0.183$). Figures 3 show

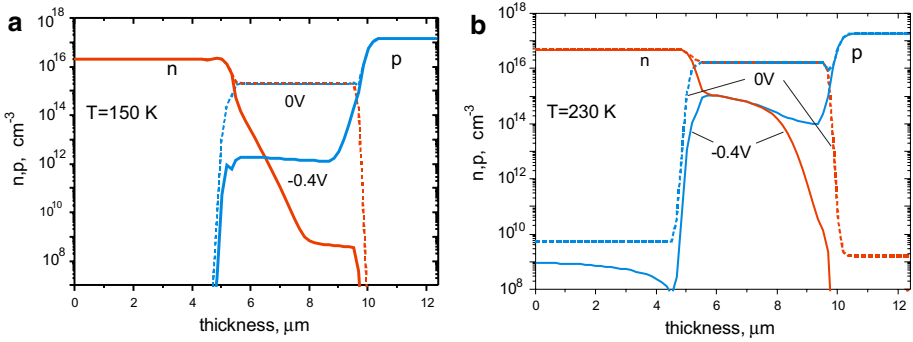


Fig. 4 Spatial distribution of electron concentration (red lines) and hole concentration (blue lines) in the analyzed structures in thermal equilibrium and after polarization with the voltage -0.4 V. (Color figure online)

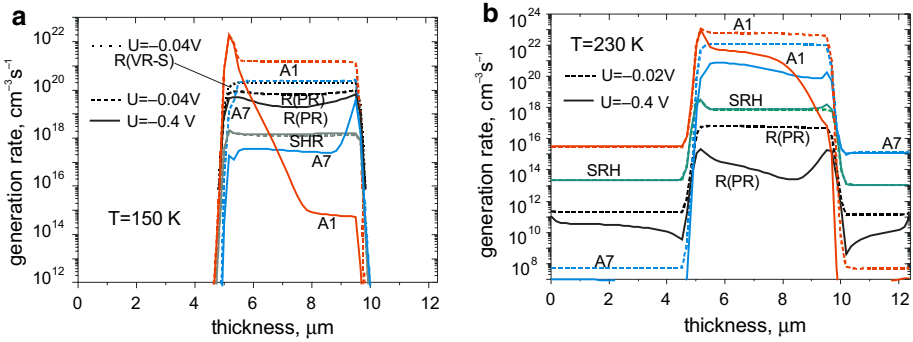


Fig. 5 Spatial distribution of generation rate determined by various G–R mechanisms. Curve denoted R(VR–S) shows the radiative generation rate expressed in the classic dependence of Van Roosbroeck and Shockley (1954)

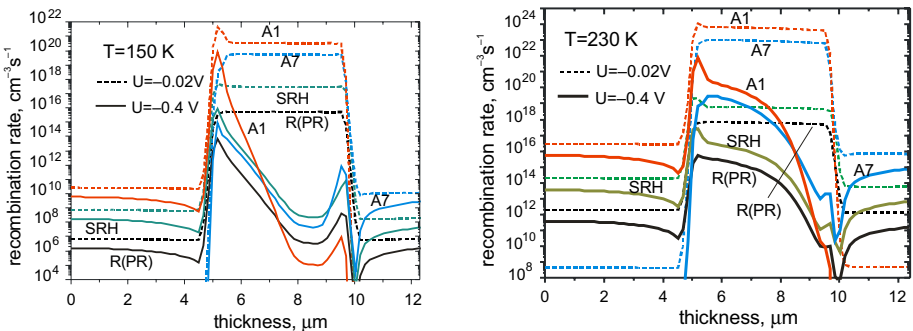


Fig. 6 Spatial distribution of recombination rate determined by various G–R mechanisms

the distribution of energy band edges in two analyzed photodiodes after biasing with reverse voltage -0.4 V (continuous lines) and low voltage -0.02 V (dashed lines). Built-in electric field causes the extraction and exclusion of electrical charge carriers

from the absorber area. This phenomenon is seen in Fig. 4. Exclusion and extraction of charge carriers is the reason of suppressing of thermal generation and recombination. Thermal generation rate determined by the mechanisms A1, A7, R and SRH is shown in Fig. 5. Strong polarization in the reverse direction (solid lines) strongly suppresses all mechanisms except for SRH processes. In the case of mechanism R, the theory of Van Roosbroeck–Shockley gives results significantly overstated when we do not consider the change in photons density when the diode is polarized. Polarization in the reverse direction suppresses recombination much stronger than generation. The rate of recombination is more strongly dependent on the concentration of carriers than the generation rate (Kopytko and Jóźwikowski 2015; Jóźwikowski et al. 2010). NEMO gives effects like strong cooling. Instead of using expensive and cumbersome cryogenic cooling, it is enough to use now much cheaper and more convenient to use thermoelectric coolers.

Figure 7 show the spatial distribution of photon density with energy greater than the width of the absorber energy gap in thermal equilibrium. Photon density at equilibrium is $2.356 \times 10^7 \text{ cm}^{-3}$ at 150 K, and $7.7 \times 10^8 \text{ cm}^{-3}$ at 230 K. Polarization in the reverse direction reduces the density of photons, especially in the absorber. It is associated with a significant reduction in radiative recombination, which is a source of photons, due to the reduction of electrons and holes concentrations. Even a small polarization in the direction of conduction has the opposite effect. In the absorber area, the concentration of carriers

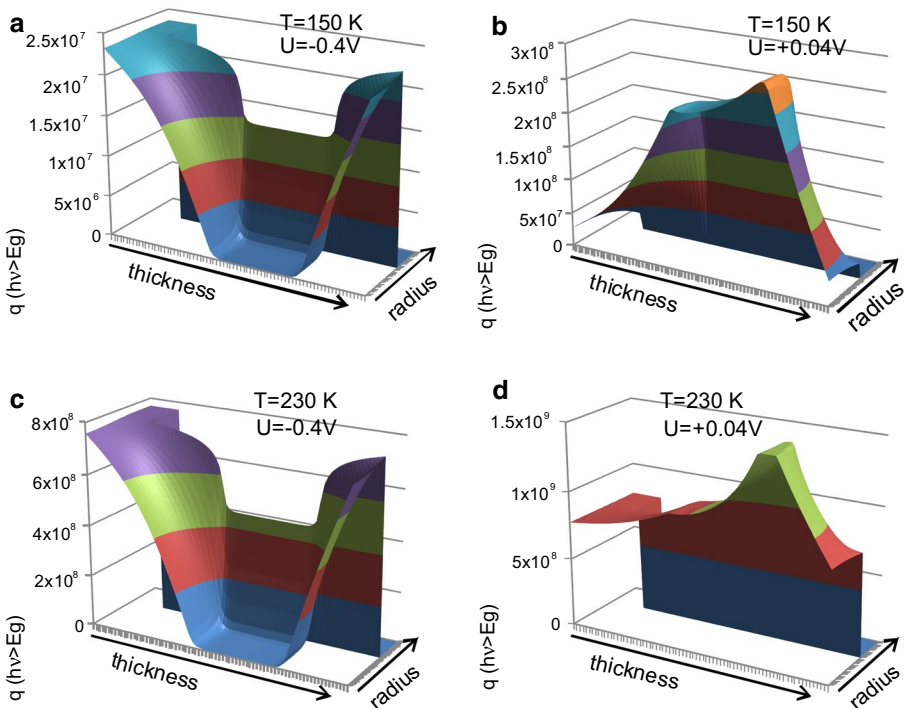


Fig. 7 Spatial distribution of photon in epitaxial layers after biasing

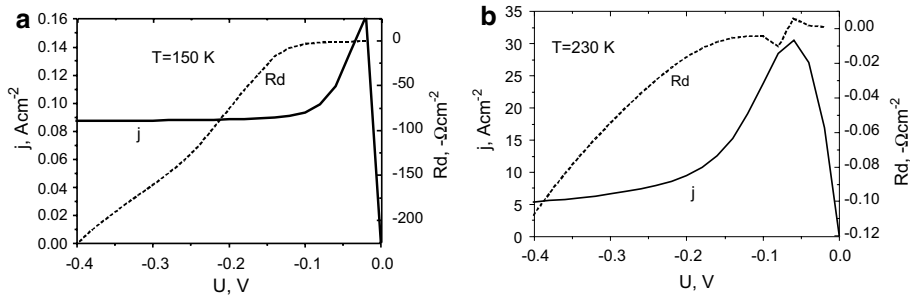


Fig. 8 Normalized (up to the upper pixel surface equal to 1 cm^2) current–voltage characteristics (solid line) and normalized dynamic resistance (dashed line) for photodiodes

increases, contributing to the increase of radial recombination. Thus, we can observe that there is a strong coupling between the concentration of carriers and the density of photons.

Figure 8 show the normalized current–voltage characteristics and normalized dynamic resistances of both photodiodes. After polarization in the reverse direction, the current rapidly increases and reaches the maximum value for a voltage of about 20 mV at 150 K and about 50 mV at 230 K. It then decreases with increasing voltage. This is explained by the effect of exclusion and extraction of carriers causing an increase in resistivity in the absorber area. Decreasing the concentration of carriers due to the phenomenon of exclusion and extraction causes an increase in resistivity of the photodiodes. This in turn reduces the current despite the voltage increase and is the cause of the negative dynamic resistance. The resistance in the absorber area determines the total resistance of the diodes. The dynamic resistance of the diode at 150 K is at least 3 orders of magnitude higher than at 230 K. Thus, reducing the temperature by 80 K (which is easily achieved by using multi-stage thermoelectric coolers) gives a possibility of significantly increasing the voltage sensitivity. The combination of NEMO with additional thermoelectric cooling is therefore a very good engineering solution that allows achieving high sensitivities without the need for cryogenic cooling. We showed in earlier works (Jóźwikowski 2017) that the effect of suppression of Auger processes reduces the G–R noise dominating in classic long-wave HgCdTe photodiodes. Both at 150 K

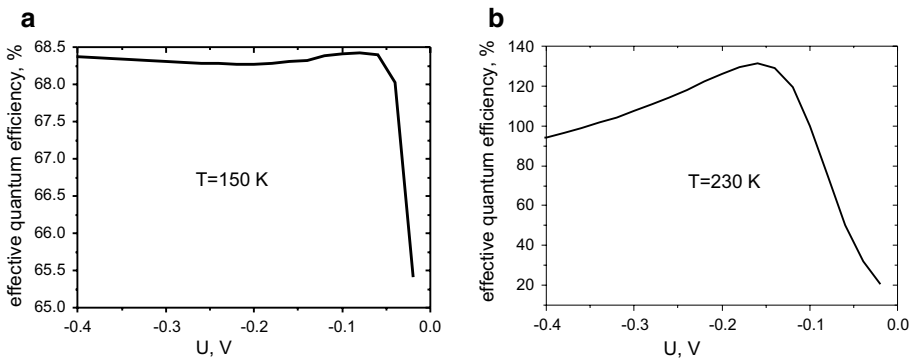


Fig. 9 Effective quantum efficiency as a function of diode bias voltage

and at 230 K the quantum efficiencies for radiation with a wavelength $\lambda = 10.6 \mu\text{m}$ are high (Fig. 9). For both photodiodes, the maximum quantum efficiency occurs for voltages slightly above 0.1 V. The initial rapid growth is associated, especially for the diode in 230 K, with an increase in the absorption coefficient (reduction in the concentration of carriers reduces the Burstein-Moss effect). The second effect increasing the effective quantum efficiency is the photoelectric gain. At 230 K, due to the photoelectric gain, effective quantum efficiency reaches values above 100%.

3 Optical cross-talk

When the detectors form matrices with densely packed elements, there are problems connected with the possibility of generating false signals in pixels adjacent to the pixel in which the photoelectric signal is generated. This phenomenon is divided into the electric cross-talk and the optical cross-talk according to the generation method of a false signal. In the first case, the change in the current within the illuminated pixel causes a parasitic change of current in neighboring pixels. In the second case, the illuminated pixel becomes a source of light, mainly due to radiative recombination. It illuminates neighboring pixels and produces there a false optical signal. This phenomenon is not particularly dangerous in matrices consisting of standard photodiodes or photoresistors, where the parasitic radiation reaches the order of single percentages of the signal photon flux. However, in the case of avalanche photodiodes, this phenomenon is very dangerous for their proper operation (Niclass et al. 2005; Rech et al. 2008). The electric cross-talk was widely studied (D’Orsogna et al. 2008, Vallone et al. 2014, 2018). Recently, works on the phenomenon of the optical cross-talk were mainly concerning the avalanche photodiodes. For the analysis of the phenomenon, researchers most often use commercial programs modeling the propagation of the light rays in the semiconductor structure. In our analysis we used a set of

Fig. 10 A diagram of a matrix of detectors. The selected area of the pixel A (pixel with height h and width l) is illuminated by the neighboring surface S of the pixel B

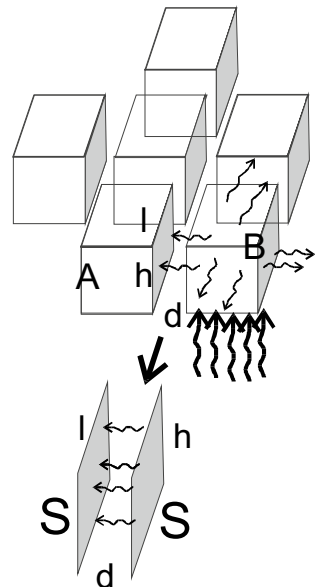
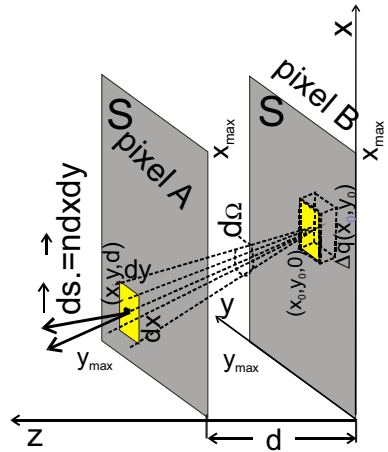


Fig. 11 The stream of light reaching from a small surface element $dA_0 = dx_0dy_0$ of the pixel B to a surface element $dA = dxdy$ of the pixel A lies in the solid angle $d\Omega$



Eqs. (1)–(8). Below, we present a sketch of our method of calculating the optical signal generated in a pixel because of the optical cross-talk phenomenon. The phenomenon concerns an adjacent pair of pixels.

The parasitic non-equilibrium radiation arises mainly because of the radiative recombination of non-equilibrium carriers generated in pixel B by the radiation absorbed in it, which is to be detected. The distance between the nearest pixels is d (Fig. 10). Figure 11 shows the method of calculating the light stream coming from a small surface element $dA_0 = Fdx_0dy_0$ of the pixel B to a small surface element $dA = dxdy$ of the pixel A. The solid angle $d\Omega$ under which the element with the area $dA = dxdy$ is visible from the point with coordinates $(x_0, y_0, 0)$ (the central point of surface element dA_0), is equal to

$$d\Omega = \frac{dxdy \cos\alpha}{r^2} = d \frac{dxdy}{\left[(x - x_0)^2 + (y - y_0)^2 + d^2 \right]^{3/2}} \tag{9}$$

The probability that the radiation emitted from a small surface element dx_0dy_0 of the pixel B reaches the surface S of the pixel A is

$$P = \frac{1}{2\pi} \int_0^{x_{MAX}} \int_0^{y_{MAX}} d \frac{dxdy}{\left[(x - x_0)^2 + (y - y_0)^2 + d^2 \right]^{3/2}} \tag{10}$$

If $\Delta q(x_0, y_0)$ is the change in photon density due to the illumination of the pixel B, in the small volume element bordering the surface S of the pixel B, the total photon current (number of photons per unit time) reaching from the surface S of the pixel B to the surface S of the pixel A is:

$$I = \frac{1}{2\pi} \frac{1}{4} c \int_0^{x_{MAX}} dx_0 \int_0^{y_{MAX}} dy_0 \int_0^{x_{MAX}} \int_0^{y_{MAX}} d \frac{\Delta q(x_0, y_0) dxdy}{\eta^3(x_0, y_0) \left[(x - x_0)^2 + (y - y_0)^2 + d^2 \right]^{3/2}} \tag{11}$$

Fig. 12 Pixels of the mesa type with cylindrical symmetry are replaced with square pixels with the same upper and lateral surfaces

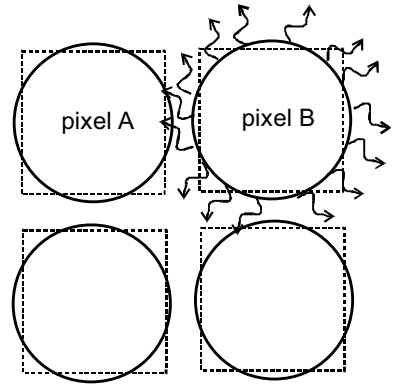
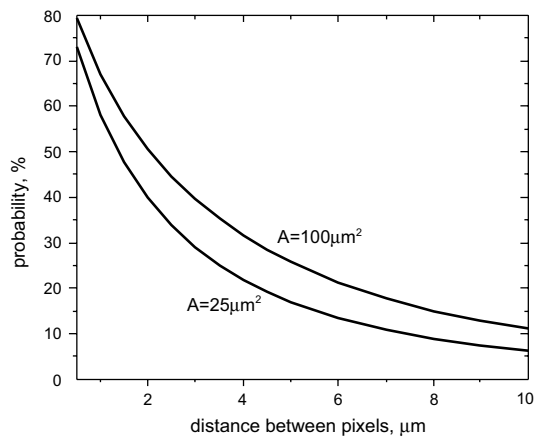


Fig. 13 Probability that the radiation from the surface S of the pixel B will reach the surface S of the pixel A as a function of the distance between pixels. A is the pixel area. The probability was calculated based on the assumption that the density of photons in the area near the lateral surface is evenly distributed



In our simulations, we most often analyze structures with cylindrical geometry. This allows solving the problem in 3D geometry using algorithms for two-dimensional problems. The results of the calculations are not much different from those one would get when solving the three-dimensional problems for square pixels with identical upper and lateral surfaces as for the cylindrical pixels. Since all physical quantities are calculated in this work for pixels with cylindrical geometry, we need to estimate them for pixels with a quadratic surface, because such matrices are most often produced in practice. By calculating the density of photons in the area near the side surface, we can determine how many photons will reach the neighboring pixel. With a good approximation, it can be assumed that potentially 25% of the photons emitted from the lateral surface of the cylinder can reach there, i.e. the current of the photons reaching (Fig. 12):

$$I' = \frac{1}{4}I. \tag{12}$$

The height of the cylindrical mesa is 11 μm, hence the height of the square mesa is 9.75 μm.

Figure 13 show the optical cross-talk understood as the percentage ratio of the photon flux emitted by the side surface of the pixel after lighting the face to the stream of photons

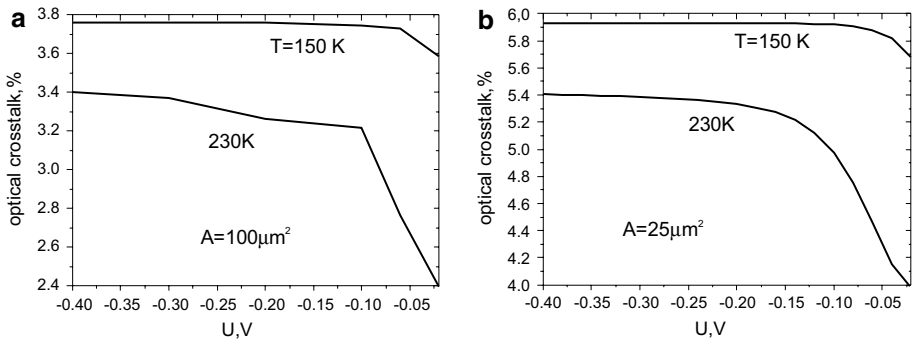


Fig. 14 Optical cross-talk due to the illumination of front surface of the pixel B. **a** Front surface equal $100\mu\text{m}^2$, **b** $25\mu\text{m}^2$

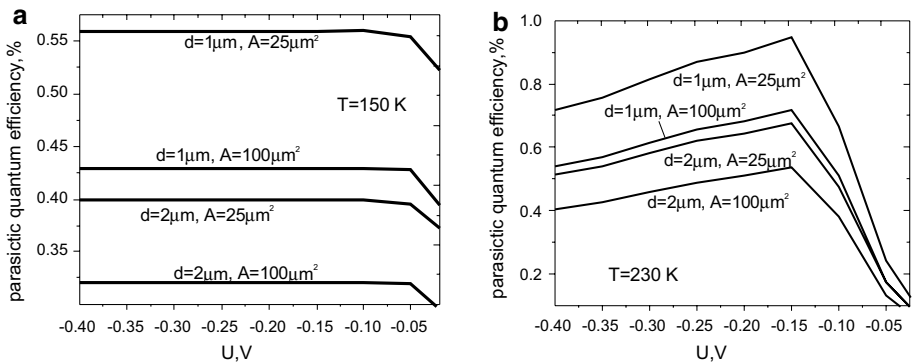


Fig. 15 The parasitic quantum efficiency in the pixel A at 150 K (**a**) and at 230 K (**b**)

illuminating the front surface. The figures show that optical cross-talk increases as the temperature and the front surface of the pixel decrease. It also grows when increasing the voltage in the blocking direction. This increase is initially quite strong and then we obtain a saturation. At 230 K, cross-talk reaches values above 3.2% for a pixel with a face area of $100\mu\text{m}^2$ and 5.2% when the surface is $25\mu\text{m}^2$. In 150 K, these values are 3.75% and 5.9%, respectively (Fig. 14).

Figure 15 show the parasitic quantum efficiency in the pixel A being the ratio of the current created in it by the effect of optical cross-talk to the stream of photons illuminating the pixel B at 230 K and at 150 K. The curves indicate the distance between adjacent pixels d and the area A of the frontal face of the pixels A. The parasitic quantum efficiency is greater in pixels with a smaller area and decreases as the distance between the pixels increases. As can be seen from Fig. 15 at the temperature of 150 K, the bias voltage in the reverse direction practically does not change the quantum efficiency starting from 50 mV. Parasitic quantum efficiency has a similar dependence on the reverse voltage as the effective quantum efficiency in the illuminated pixel. For 230 K the maximum values of parasitic quantum efficiency occur at the voltage of -0.15 V . For this voltage value, the effective quantum efficiency also obtains the maximum value (Fig. 9b).

4 Conclusion

The phenomenon of exclusion and extraction of charge carriers in combination with the photon reabsorption process reduces both the RG rate and the RR rate. Taking into account the change in photon density is necessary to correctly determine the effect of the R processes on the process of carrier and energy transport in heterostructures. The numerical method used allows to calculate the spatial distribution of photons in the heterostructure and to associate it with non-equilibrium carrier concentrations. NEMO has a significant influence on this distribution. We observe the effect of reducing the density of photons after the polarization of detectors in the reverse direction, which is caused by a significant suppression of the RR being the source of photon generation. After the polarization of the structure in the direction of conduction, the concentration of carriers increases, especially in the absorber. This causes a local increase of the RR rate and, therefore, an increase of photon generation rate, which increases their density. Figure 7 illustrate this perfectly.

We estimated the optical cross-talk in the matrix of non-equilibrium detectors with the face of the pixel $5 \times 5 \mu\text{m}^2$ and $10 \times 10 \mu\text{m}^2$. For the long wavelength infrared detectors analyzed, parasitic quantum efficiency does not exceed 1% for distances between matrix detectors equal to $1 \mu\text{m}$, which implies that this phenomenon has a marginal effect on the parameters of the matrix usage.

Acknowledgements The work has been undertaken under the financial support of the Polish National Science Centre as research Project No. DEC-2016/23/B/ST7/03958.

Open Access This article is distributed under the terms of the Creative Commons Attribution 4.0 International License (<http://creativecommons.org/licenses/by/4.0/>), which permits unrestricted use, distribution, and reproduction in any medium, provided you give appropriate credit to the original author(s) and the source, provide a link to the Creative Commons license, and indicate if changes were made.

References

- D'Orsogna, D., Tobin, S.P., Bellottil, E.: Numerical analysis of a very long-wavelength HgCdTe pixel array for infrared detection. *J. Electron. Mater.* **37**, 1349–1355 (2008). <https://doi.org/10.1007/s11664-008-0438-z>
- Humphreys, R.G.: Radiative lifetime in semiconductors for infrared detection. *Infrared Phys.* **23**, 171–175 (1983)
- Humphreys, R.G.: Radiative lifetime in semiconductors for infrared detection. *Infrared Phys.* **26**, 337–342 (1986)
- Jóźwikowski, K.: Langevin-like method for modelling the noise currents in HgCdTe barrier LWIR detectors. *Opt. Quantum Electron.* **49**, 101 (2017). <https://doi.org/10.1007/s11082-017-0926-6>
- Jóźwikowski, K., Kopytko, M., Rogalski, A., Jóźwikowska, A.: Enhanced numerical analysis of current-voltage characteristics of long wavelength infrared n-on-p HgCdTe photodiodes. *J. Appl. Phys.* **108**, 074519 (2010). <https://doi.org/10.1063/1.3483926>
- Jóźwikowski, K., Kopytko, M., Rogalski, A.: Numerical estimations of carrier generation-recombination processes and photon recycling effect in 3- μm n-on-p HgCdTe photodiodes. *Opt. Eng.* **50**, 061003 (2011). <https://doi.org/10.1117/1.3572167>
- Jóźwikowski, K., Kopytko, M., Rogalski, A.: Numerical estimations of carrier generation-recombination processes and the photon recycling effect in HgCdTe heterostructure photodiodes. *J. Electron. Mater.* **41**, 2766–2774 (2012). <https://doi.org/10.1007/s11664-012-2093-7>
- Jóźwikowski, K., Jóźwikowska, A., Nietopiel, M.: The non-equilibrium statistical distribution function for electrons and holes in semiconductor heterostructures in steady-state conditions. *Entropy* **17**, 4110–4133 (2015). <https://doi.org/10.3390/e17064110>

- Jóźwikowski, K., Jóźwikowska, A., Nietopiel, M.: The numerical method for solving the transport equations in HgCdTe heterostructures using the non-equilibrium distribution functions. *Opt. Quantum Electron.* **49**, 98 (2017a). <https://doi.org/10.1007/s11082-017-0923-9>
- Jóźwikowski, K., Piotrowski, J., Jóźwikowska, A., Kopytko, M., Martyniuk, P., Gawron, W., Madejczyk, P., Kowalewski, A., Markowska, O., Martyniuk, A., Rogalski, A.: The numerical-experimental enhanced analysis of HOT MCT barrier infrared detectors. *J. Electron. Mater.* **46**, 5471–5478 (2017b). <https://doi.org/10.1007/s11664-017-5513-x>
- Kopytko, M., Jóźwikowski, K.: Generation–recombination effect in MWIR HgCdTe barrier detectors for high-temperature operation. *IEEE Trans. Electron Dev.* **62**, 2278–2284 (2015). <https://doi.org/10.1109/TED.2015.2430527>
- Niclass, C., Rochas, A., Besse, P.-A., Charbon, E.: Design and characterization of a CMOS 3-D image sensor based on single photon avalanche diodes. *IEEE J. Solid State Circuits* **40**, 1847–1854 (2005). <https://doi.org/10.1109/JSSC.2005.848173>
- Rech, I., Ingargiola, A., Spinelli, R., Labanca, I., Marangoni, S., Ghioni, M., Cova, S.: A new approach to optical crosstalk modeling in single-photon avalanche diodes. *IEEE Photonics Technol. Lett.* **20**, 330–332 (2008). <https://doi.org/10.1109/LPT.2007.915654>
- Vallone, M., Goano, M., Bertazzi, F., Ghione, G., Wollrab, R., Ziegler, J.: Modeling photocurrent spectra of single-color and dual-band HgCdTe photodetectors: Is 3D simulation unavoidable? *J. Electron. Mater.* **43**, 3070–3076 (2014). <https://doi.org/10.1007/s11664-014-3252-9>
- Vallone, M., Goano, M., Bertazzi, F., Ghione, G., Hanna, S., Eich, D., Figgemeyer, H.: Diffusive-probabilistic model for inter-pixel crosstalk in HgCdTe focal plane arrays. *IEEE J. Electron. Dev. Soc.* **6**, 664–673 (2018). <https://doi.org/10.1109/JEDS.2018.2835818>
- Van Roosbroeck, W., Shockley, W.: Photon-radiative recombination of electrons and holes in Germanium. *Phys. Rev.* **94**(6), 1558–1560 (1954)

Publisher's Note Springer Nature remains neutral with regard to jurisdictional claims in published maps and institutional affiliations.